Dear author,

In the stage of preparing your full work for evaluation, after receiving approval of the corresponding abstract, we kindly ask you to follow the next steps:

1. Update your approved abstract (you might want to introduce modifications) and submit it now in a written version according to the abstract template (many abstracts were introduced directly into the websystem). This version of the abstract will compose the abstracts booklet to be distributed to the participants when registering;

2. Fill the form in the next page, indicating to which section you would like your work to be directed. This will help organizing the sessions according to the mini-symposia advertised rather than in the areas and subareas present in the websystem. We apologize for this possible confusion. The reason is that we are using the websystem provided by ABCM, which does not allow us to introduce thematic sessions freely.

If any doubts arise, please contact us. Your presence in MecSol 2017 will help making this a very successful event. We look forward to seeing you in Joinville!

With kind regards,

The Organizing Committee
MecSol 2017

6 th International Symposium on Solid Mechanics

Select the box to select the Mini-Symposia:

[ ] Multiaxial and Fretting Fatigue (Edgar Mamiya and Lucival Malcher);

[ ] Composite Materials (Ricardo de Medeiros);

[ ] Constitutive Models I - Plasticity and Damage (Lucival Malcher, Miguel Vaz Jr. and Edgar Mamiya);

[ ] Constitutive Models II - Viscoelastic and Viscoplastic Solids: Models and Applications (Heraldo Mattos);

[ ] Impact Engineering (Marcílio Alves);

[ ] Structural Reliability Methods and Reliability-Based Design Optimization (André Beck);

[X] Topology Optimization of Multifunctional Materials, Fluids and Structures (Eduardo Lenz Cardoso e Emilio Carlos Nelli Silva);

[ ] Topological Derivatives: Theory and Applications (André Novotny);

[ ] X-FEM, G-FEM and Meshfree Methods (Roberto Dalledone Machado and Rodrigo Rossi);

[ ] High Order Finite Elements (Marco Lúcio Bittencourt);

[ ] Nonlinear Analyses (Eduardo Campello);

[ ] Other section;

MECSOL Joinville 2017
April 26-28, 2017
Joinville, Santa Catarina, Brazil

OPTIMAL DISTRIBUTION OF A HOLLOW SPHERE MATERIAL APPLIED TO THE DESIGN OF THREE DIMENSIONAL STRUCTURE WITH MINIMUM VOLUME CONSIDERING STRESS CONSTRAINTS

Bruno Guilherme Christoff
Department of Mechanical Engineering
Santa Catarina State University
brunogch@gmail.com

Luiz Fernando Santos Souza
Department of Mechanical Engineering
Santa Catarina State University
luiz03fernando11@gmail.com

Eduardo Lenz Cardoso
Department of Mechanical Engineering
Santa Catarina State University
eduardo.cardoso@udesc.br

Ricardo de Medeiros
Department of Mechanical Engineering
Santa Catarina State University
ricardo.medeiros@udesc.br

ABSTRACT

This work describes a methodology to design optimal lightweight structures comprised of a hollow-sphere cellular material. The objective is to minimize the structural volume while respecting strength limits associated to this specific type of micro structure. The effective elastic properties of the cellular material are obtained by means of the homogenization by asymptotic expansion and the failure criteria is the well-known Tsai-Wu stress criteria. Computational simulation, by using commercial software, is carried out to simulate mechanical testing using a hollow sphere material in order to obtain the limit average macroscopic stresses. Thus, by varying the geometrical parameters of the hollow spheres it is possible to adjust equations relating the effective properties of the media to these parameters, as well as equations relating the strength parameters. The Augmented Lagrangian method is used in order to solve the constrained problem and as optimization solver, a modified descent direction algorithm is adopted. The results show that the optimal distribution of hollow spheres is consistent with the expected material distribution.

Keywords: Cellular materials, Hollow sphere structures, Topology optimization

1. INTRODUCTION

Hollow sphere structures are a novel lightweight microstructure in the class of cellular materials. The engineering application of such kind of material has been growing extensively in the past years, encouraging the research on this particular area of solid mechanics.

This kind of material can be used in order to provide very specific characteristics, such as a good thermal insulation, the potential to absorb high amounts of energy, besides being able to being used for noise control and vibration damping. [1]

A crucial factor that makes this a very unique class of material is that they can be manufactured from a broad range of materials and can be assembled in a periodic structure with a relatively small amount of imperfections. [2]

Despite the large number of works concerning aspects such the thermal conductivity of hollow sphere structures, few can be found in a structural context. Since this material can be used as a multifunctional material, the motivation of this work is to address the mechanical behaviour, using a linear elastic consideration, of this kind of structure and its optimization. This opens a possibility of the use of this kind of material, for instance, for thermal applications and simultaneously as a structural component.

1.1 Outline

The present work aims to develop an optimization algorithm in order to obtain the optimal distribution of hollow spheres in a given domain in order to minimize its volume, respecting a local stress constraint. A preliminary study is made by using a cantilever beam as example and to show the consistency of the algorithm.

It is considered that the mechanical behaviour of every finite element of the mesh is described by a pair of geometrical parameters, the inner and outer diameters of a hollow sphere. By using the homogenization by asymptotic expansion it is possible to find the effective elasticity properties of a media formed by this kind of material. By varying these geometrical parameters, equations relating the effective fourth order elasticity tensor to the geometrical parameters are obtained.

The phenomenological Tsai-Wu stress criteria is used as failure criteria. The strength parameters of the method are obtained through a commercial software and, as for the elastic constants, equations relating the strength parameters to the geometrical parameters of the hollow spheres are obtained.

The volume of the structure is considered as objective function and as constraint, every element of the mesh must satisfy the Tsai Wu failure criteria. The Augmented Lagrangian method is used to solve the constrained problem.

To this end, this work is organized as follows:

- The main concepts used for the determination of the effective properties of a cellular material are presented. The model used to describe the material model is shown as well as the finite element discretization used in order to obtain the elastic properties of the media. The Tsai Wu failure criteria is briefly explained and the model adopted to obtain the strength parameters is shown;

- The formulation of the optimization problem is addressed. The objective function and the constraint are presented. The derivatives of the Augmented Lagrangian function in regard to the design variables are obtained;

- The preliminary result is presented and discussed;

- The main conclusions.

2. Properties

The effective properties of the hollow sphere structure are obtained through the homogenization by asymptotic expansion and the strength parameters were obtained using a commercial software.

The model adopted to describe the representative volume element is shown in figure 1, in which two adjacent spheres are connected by a flat area. This model has two geometrical parameters, the outer diameter ρ_o and the inner diameter ρ_i and the flat area is a function of both diameters.

Figure 1. Representation of the hollow sphere model (cross section).

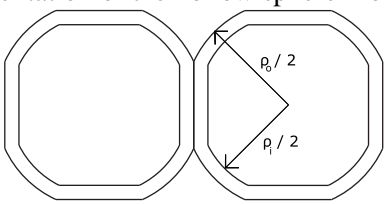

2.1 Elastic Properties

In the context of linear elasticity, the effective properties of a periodic media can be found by using the homogenization by asymptotic expansion in two or more scales. This method is based on the assumption that a base cell, or representative volume element (RVE) repeats itself periodically in the whole domain. This method allows to obtain the macroscopic of a heterogeneous media by analysing only the cell domain, requiring much less computational effort to solve the problem. As shown by [3], the effective properties of composites with a periodic structure are better approximated using the homogenization by asymptotic method rather than other theories presented in the literature.

This method follows three basic considerations [4]. The first one divides the problem into a macroscopic and a microscopic scale. Both scales are related by a small parameter ε in the form

$$\boldsymbol{y} = \frac{\boldsymbol{x}}{\varepsilon}, \tag{1}$$

where $\boldsymbol{x}$ and $\boldsymbol{y}$ are, respectively, the coordinates into the macroscopic and microscopic levels, rendering the microscopic scale very small regarding the macroscopic scale. The second one demands that the displacement field of the media can be written in an asymptotic expansion form as

$$\boldsymbol{u}^{\varepsilon}(\boldsymbol{x},\boldsymbol{y}) = \boldsymbol{u}^{0}(\boldsymbol{x},\boldsymbol{y}) + \varepsilon \boldsymbol{u}^{1}(\boldsymbol{x},\boldsymbol{y}) + \varepsilon^{2}\boldsymbol{u}^{2}(\boldsymbol{x},\boldsymbol{y}) + \ldots, \tag{2}$$

where $\boldsymbol{u}^{\varepsilon}$ is the total displacement field and $\boldsymbol{u}^{0}$, $\boldsymbol{u}^{1}$ and $\boldsymbol{u}^{2}$ are the contributions on the displacement of the media of the macroscopic scale, microscopic scale and eventually smaller scales. The third one demands that the displacements on the boundaries of the RVE are periodic, rendering the displacement field on opposite sides the same.

The theoretical background of the method is well established in the literature [5], [6], [7]. A general elasticity problem consist in, basically, finding a characteristic displacement field, $\boldsymbol{\chi}$, by using

$$\int_{\boldsymbol{Y}} C_{ijpq} \frac{\partial \chi_p^{kl}}{\partial y_q} \frac{\partial v_i}{\partial y_j} d\boldsymbol{Y} = \int_{\boldsymbol{Y}} C_{ijkl} \frac{\partial v_i}{\partial y_j} d\boldsymbol{Y}, \tag{3}$$

where $\boldsymbol{C}$ is the fourth order elasticity tensor of the base material, $\boldsymbol{Y}$ is the vector containing the dimensions of the base cell, $\boldsymbol{y}$ is the position vector in the microscopic level and $\boldsymbol{v}$ is a virtual displacement. The periodic displacement field is used in

$$C_{ijkl}^{H} = \frac{1}{|\boldsymbol{Y}|} \int_{\boldsymbol{Y}} \left(C_{ijkl} - C_{ijpq} \frac{\partial \chi_p^{kl}}{\partial y_q} \right) d\boldsymbol{Y}, \tag{4}$$

where $\boldsymbol{C}^H$ is the homogenized fourth order elasticity tensor, in order to find all the 21 elastic constants of the media. The indexes i, j, k, p, q and l can assume values between 1 and 3 and, in order to obtain all the elastic constants, the characteristic displacement field must be found for the cases $kl = 11$, $kl = 22$, $kl = 33$, $kl = 12$, $kl = 23$ and $kl = 13$.

2.1.1 Effective Elasticity Properties

For the determination of the homogenized fourth order tensor, a computational code based on the finite element method was written in order to solve the integral equations shown in the previous section. The numerical development of the homogenization by asymptotic method can be found in [8] and [9].

The element used in the discretization is the Trilinear Isoparametric Hexahedral Element with incompatible modes. As shown by [10], the addition of the incompatible modes increases the accuracy of both displacement and stress fields. Also, this element does not affect the assembly of the global stiffness matrix compared with usual Hexahedral element, since the sizes of the local matrices, for both cases, are the same.

An unitary cube is considered for the domain and, for sake of simplicity, the whole domain is divided into a structured finite element mesh and a interpolation scheme is adopted in order to set the properties for both void and solid elements. A constant centroidal value, ρ_v, is associated to every element of the mesh as,

$$\boldsymbol{C}^e = \rho_v^e \boldsymbol{C}^0, \tag{5}$$

where $\boldsymbol{C}^e$ is the effective property of the e-th element of the mesh, $\boldsymbol{C}^0$ is the base material property and ρ_v^e is a pseudo density associated to the e-th element of the mesh. For a solid element, the pseudo density assumes an unitary value, rendering the property of this element the property of the base material. For a void element, the pseudo density assumes a vary small value, rendering the influence of this element on the assembly of the global matrices negligible.

The finite element model used to discretize the RVE is shown in figure 2, in which the whole base cell is shown in the right and a cross section is shown in the left. The void elements were suppressed for the visualization. A mesh of $100 \times 100 \times 100$ elements was chosen after a proper convergence analysis.

Figure 2. Finite element model. Entire RVE (left). Cross section (right).

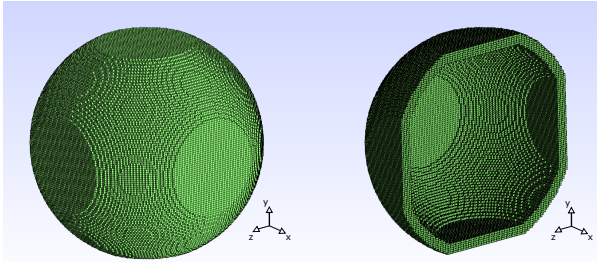

As base material, an aluminium alloy was chosen, since this material is commonly used in rapid prototyping processes [11]. The properties used are shown in table 1.

Table 1. Mechanical properties of the base material (Aluminium)

Young Modulus [GPa]	70.0
Poisson	0.33
Void Density	0.001
Yield Strength [MPa]	240.0

By varying the geometrical parameters of the model, it is possible to set an equation relating them to an effective property of the media formed by the repetition of hollow spheres. The range adopted in this work is

$$\begin{array}{ccccc} 1.09 & \leq & \rho_o & \leq & 1.2 \\ \rho_o - 0.2 & \leq & \rho_i & \leq & \rho_0 - 0.01, \end{array} \tag{6}$$

in which the RVE has unitary dimension. For all combinations of parameters, the homogenized constitutive tensor has the form

$$\boldsymbol{C}^H = \begin{bmatrix} C^H_{1111} & C^H_{1122} & C^H_{1133} & 0 & 0 & 0 \\ & C^H_{2222} & C^H_{2233} & 0 & 0 & 0 \\ & & C^H_{3333} & 0 & 0 & 0 \\ & & & C^H_{1212} & 0 & 0 \\ & & & & C^H_{2323} & 0 \\ sym. & & & & & C^H_{1313}, \end{bmatrix} \tag{7}$$

where $C^H_{1111} = C^H_{2222} = C^H_{3333}$, $C^H_{1122} = C^H_{1133} = C^H_{2233}$ and $C^H_{1212} = C^H_{1313} = C^H_{2323}$. The shear components can not be related to the normal and coupled components, which indicates a cubic symmetry on the tensor.

As an optimization procedure is addressed and a gradient method was chosen, a continuous equation must be found to adjust the discrete set of points obtained in the simulations. Thus, the least square method is used to adjust a polynomial function to these points and the relations obtained are

$$\begin{aligned} C^H_{1111}(\rho_i, \rho_o) &= 216.82{\rho_o}^3 - 20.83\rho_i{\rho_o}^2 - 348.38{\rho_o}^2 - 588.11{\rho_i}^2\rho_o + 847.58\rho_i\rho_o - 183.31\rho_o \\ &+ 326.72{\rho_i}^3 - 266.65{\rho_i}^2 - 92.39\rho_i + 108.94\,[GPa], \end{aligned} \tag{8}$$

$$\begin{aligned} C^H_{1122}(\rho_i, \rho_o) &= 1148.55\,\rho_i{\rho_o}^2 - 671.20\,{\rho_o}^3 + 282.47\,{\rho_i}^3 + 280.89\,{\rho_i}^2 + 263.22\,\rho_i - 833.54\,\rho_i\rho_o \\ &+ 1337.64\,{\rho_o}^2 - 981.53\,{\rho_i}^2\rho_o - 1191.81\,\rho_o + 366.79\,[GPa] \end{aligned} \tag{9}$$

and

$$\begin{aligned} C^H_{1212}(\rho_i, \rho_o) &= -8.13\,{\rho_o}^3 - 2.44\,\rho_i{\rho_o}^2 + 80.76\,{\rho_o}^2 + 22.56\,{\rho_i}^2\rho_o - 117.16\,\rho_i\rho_o - 26.55\,\rho_o \\ &+ 23.46\,{\rho_i}^3 - 81.61\,{\rho_i}^2 + 157.47\,\rho_i - 48.40\,[GPa], \end{aligned} \tag{10}$$

The equation relating the volume fraction of an element to the geometrical parameters is

$$f_v(\rho_i, \rho_o) = 0.80\,{\rho_o}^2 + 0.73\,\rho_i\rho_o - 0.67\,\rho_o - 1.68\,{\rho_i}^2 + 1.00\,\rho_i - 0.19. \tag{11}$$

2.2 Strenght Properties

As it is considered that, for every finite element of the mesh, a pair of design variables is associated to, it is possible to find the fourth order elasticity tensor for all elements. With these tensors, it is possible to find the macroscopic stress field for every element of the mesh by using the standard finite element method approach. Thus, the idea is to predict if the microscopic structure related to an element of the mesh fails under a certain stress field. As a cellular material can be seen as a particularity of a composite, the phenomenological Tsa-Wu failure criteria [12] is used. In the present work, the strength parameters used in the method, generally obtained experimentally, are obtained through numerical simulation. Thus, both a tensile and a shear tests are simulated and the maximum allowed stress are obtained from the simulation.

It is considered a failure surface in the form

$$\Phi(\boldsymbol{\sigma}) = \boldsymbol{F}^T\boldsymbol{\sigma} + \boldsymbol{\sigma}^T\boldsymbol{M}\boldsymbol{\sigma}, \tag{12}$$

in which $\boldsymbol{\sigma}$ is the stress field that a given point of the domain is subjected. The failure is reached when the right hand side of this equation is equal or greater than one. $\boldsymbol{F}$ and $\boldsymbol{M}$ are strength tensors and, due to the symmetries in the model, can be written as

$$\boldsymbol{F}^T = \begin{bmatrix} F_1 & F_1 & F_1 & F_4 & F_4 & F_4 \end{bmatrix} \tag{13}$$

and

$$\boldsymbol{M} = \begin{bmatrix} M_{11} & M_{12} & M_{12} & 0 & 0 & 0 \\ & M_{11} & M_{12} & 0 & 0 & 0 \\ & & M_{11} & 0 & 0 & 0 \\ & & & M_{44} & 0 & 0 \\ & & & & M_{44} & 0 \\ sym. & & & & & M_{44} \end{bmatrix}, \tag{14}$$

in which the therms of these tensors can be written as an expression of basic strength parameters as

$$F_1 = \frac{1}{X_1^t} - \frac{1}{X_1^c}, \tag{15}$$

$$F_4 = 0, \tag{16}$$

$$M_{11} = \frac{1}{X_1^t X_1^c}, \tag{17}$$

and

$$M_{44} = \frac{1}{S^2}, \tag{18}$$

where X_1^t is the failure stress in a principal direction, X_1^c is the compressive failure stress in the same direction and S is the failure shear stress in a principal plane.

The component M_{12} can not be written in therms of these basic parameters, and, as shown in [13] it can be approximated by

$$M_{12} = -\frac{1}{2}\sqrt{M_{11}M_{22}}. \tag{19}$$

2.2.1 Numerical Model

A numerical model using a commercial finite element software was used to obtain stresses on a unit cell from a set of geometries aiming to achieve a correlation between the geometry parameters (external and internal diameters) with the stress on the top face.

The model showed in the Figure 3, consists of quadratic shell elements with 6 degrees of freedom per node (Abaqus S8R element). A convergence analysis was conducted and models with 5800 elements or more are mesh independent. Additionally, every unit cell tested had the same length ($0.5mm$). This value is used to keep the microscopic scale within 5 : 1 relative to the speciment size ($250 \times 25 \times 2.5mm$ in the ASTM D3039).

Figure 3. Computational model.

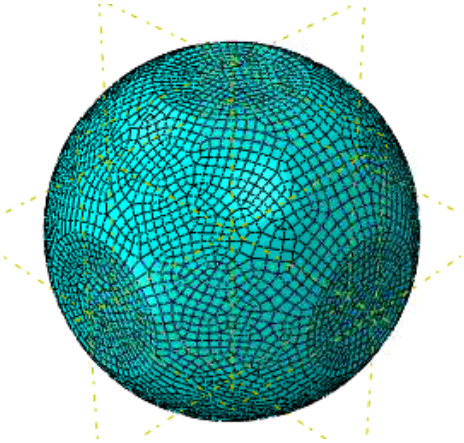

Two kinds of mechanical tests were simulated with this numerical model: a tensile test and a shear test. Furthermore, for each test, 25 different geometries were analysed covering the range for the internal and external diameters shown in equation 6.

For the tensile test, a displacement was imposed on the top surface and as boundary conditions one has the bottom face crimped and the side faces blocked its displacement in the normal direction to impose the condition of periodicity. On the other hand, the boundary conditions for the shear test were the blockage of bottom face in X direction and side faces in Y direction. Additionally, the shear loads were imposed on the top and side faces. More details about the boundary conditions and properties evaluations are extensively discussed in [14, 15, 16, 17].

For all cases addressed, an average stress, given by the total amount of force applied in the moment that any element of the model reaches the maximum tensile stress, by the area of the face of the domain is calculated. This measure, for traction, compression and shear, are the strength parameters of the Tsai Wu failure criteria. Thus, when the macroscopic stress field reaches the Tsai Wu limit, the microscopic media collapses. This can be seen as an apparent stress that, in the macroscopic domain, causes the failure in the microscopic domain. Figure 4 shows the von Mises field at the micro structure for the tensile and for the shear test.

Figure 4. Von Mises stress field obtained in the micro structure, for the tensile and for the shear test.

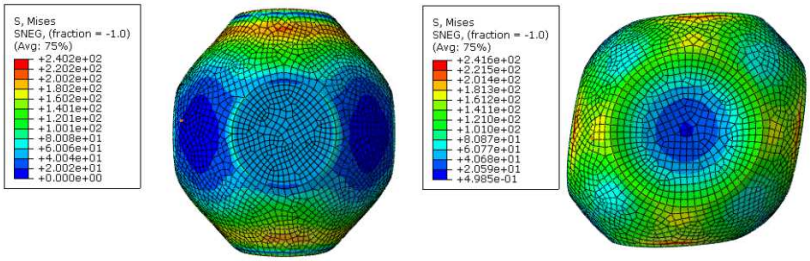

By using the least square method to adjust equations relating the geometrical parameters of the base cell to the apparent strength parameters one get

$$\begin{aligned} X_1^t(\rho_i,\rho_o) &= -621.78\rho_o^3 - 460.78\rho_i\rho_o^2 + 3265.36\rho_o^2 - 537.40\rho_i^2\rho_o + 1376.67\rho_i\rho_o - 4660.24\rho_o \\ &+ 477.78\rho_i^3 - 717.95\rho_i^2 + 168.15\rho_i + 1713.52 \end{aligned} \quad (20)$$

and

$$\begin{aligned} S(\rho_i,\rho_o) &= 2204.09\rho_o^3 - 609.49\rho_i\rho_o^2 - 6558.69\rho_o^2 - 646.36\rho_i^2\rho_o + 2228.93\rho_i\rho_o + 6280.75\rho_o \\ &+ 398.11\rho_i^3 - 317.90\rho_i^2 - 935.77\rho_i - 2047.62. \end{aligned} \quad (21)$$

In this work the strength properties on traction and compression are considered the same. In order to model a consistent compressive behaviour of this kind of micro structures, a nonlinear compressive test should be performed.

3. Formulation

This section presents the main considerations concerning the optimization procedure.

The finite element method is used in order to obtain the equilibrium of the problem, as well as the stress field. The Trilinear Isoparametric Hexahedral Element with incompatible modes is used.

The volume of the structure is chosen as objective function and, for every element of the finite element mesh, a stress constraint, evaluated at its centroid, is associated. This constrained optimization problem is solved by using the Augmented Lagrangian method, which consists in solving sequential unconstrained problems. This method adds a penalty factor and Lagrange multipliers to the objective function that, when the unconstrained problem reaches its minimum (internal loop), are updated (external loop) following a certain rule.

The adjoint method is used to evaluate the derivatives of the Augmented Lagrangian function in order to avoid the determination of the derivatives of the displacement field with respect to the design variables.

3.1 Optimization definitions

The objective function is given by

$$\sum_{e=1}^{n} V_e f_v^e(\boldsymbol{\rho}), \tag{22}$$

where f_v^e is the volume fraction of the e-th element of the mesh, $\boldsymbol{\rho}$ is the vector of design variables, the inner and outer diameters associated to every element of the mesh and n is the total number of elements.

Every element of the mesh must satisfy a local constraint, namely,

$$\Phi_e(\boldsymbol{\rho}) \leq 1 \qquad e = 1,\ldots,n, \tag{23}$$

where Φ_e is the Tsai Wu failure criteria of the e-th element of the mesh.

Thus, the optimization problem can be set as

$$\begin{aligned} &\underset{\boldsymbol{\rho}}{\text{Minimize}} \quad \sum_{e=1}^{n} V_e f_v^e(\boldsymbol{\rho}) \\ &\text{Subject to} \quad \Phi_e(\boldsymbol{\rho}) \leq 1 \end{aligned} \tag{24}$$

with design variables respecting the side constraints presented in equation 6.

The Augmented Lagrangian function, herewith the adjoint method is given by

$$\mathscr{L}(\boldsymbol{\rho}) = \sum_{e=1}^{n} V_e f_v^e(\boldsymbol{\rho}) + \sum_{e=1}^{n} \frac{r}{2} \langle \frac{\mu_e(\boldsymbol{\rho})}{r} + \Phi_e(\boldsymbol{\rho}) - 1 \rangle^2 + \boldsymbol{\lambda}^T (\boldsymbol{K}(\boldsymbol{\rho})\boldsymbol{U}(\boldsymbol{\rho}) - \boldsymbol{P}), \tag{25}$$

where r is a penalty parameters, μ_e is the Lagrange Multiplier associated to the e-th element of the mesh, $\boldsymbol{\lambda}$ is the adjoint vector, $\boldsymbol{K}$ is the global stiffness matrix, $\boldsymbol{U}$ is the displacement field and $\boldsymbol{P}$ is the load vector.

A basic density filtering scheme [18] is adopted. The design variables attached to an element e are related to the variables of its neighbours as

$$N_e = \left\{ j, \| \boldsymbol{c}_j - \boldsymbol{c}_e \| \leq R \right\}, \tag{26}$$

where $\boldsymbol{c}_j$ is the centroid of the element j, $\boldsymbol{c}_e$ is the centroid of the element e and R is a predefined filtering radius. The dependency of the design variable to its neighbours can be post as

$$\tilde{\rho}_e = \frac{\sum_{j\in N_e} w\left(\boldsymbol{c}_j\right) V_j \rho_j}{\sum_{j\in N_e} w\left(\boldsymbol{c}_j\right) V_j} \tag{27}$$

where $w\left(\boldsymbol{c}_j\right)$ is a linear decaying weighting function [19].

As optimization solver, the method proposed by [20] is used.

3.2 Sensitivity analysis

The derivatives of the Lagrangian Function, with respect to the m-th design variable is given by

$$\frac{d\mathscr{L}}{d\rho_m} = \sum_{e=1}^{n} V_e \frac{df_e(\boldsymbol{\rho})}{d\rho_m} + \sum_e r\left\langle \frac{\mu_e}{r} + \Phi_e - 1 \right\rangle \frac{d\Phi_e}{d\rho_m} + \boldsymbol{\lambda}^T \frac{d\boldsymbol{K}}{d\rho_m}\boldsymbol{U} + \boldsymbol{\lambda}\boldsymbol{K}\frac{d\boldsymbol{U}}{d\rho_m}, \tag{28}$$

where the derivatives of the Tsai Wu failure criteria are

$$\frac{d\Phi_e}{d\rho_m} = \frac{d\boldsymbol{F}_e^T}{d\rho_m}\boldsymbol{\sigma}_e + \boldsymbol{F}_i^T\frac{d\boldsymbol{\sigma}_e}{d\rho_m} + 2\boldsymbol{\sigma}_e^T\boldsymbol{M}_e\frac{d\boldsymbol{\sigma}_e}{d\rho_m} + \boldsymbol{\sigma}_e^T\frac{d\boldsymbol{M}_e}{d\rho_m}\boldsymbol{\sigma}_e. \tag{29}$$

The derivatives of the strength tensors $\boldsymbol{F}$ and $\boldsymbol{M}$ can be obtained directly by equations 20 and 21. The stress field is calculated by the usual finite element form in the centroid of the element and its derivatives are given by

$$\frac{d\boldsymbol{\sigma}_e}{d\rho_m} = \frac{d\boldsymbol{C}_e^H}{d\rho_m}\boldsymbol{B}_e\boldsymbol{A}_e\boldsymbol{H}_e\boldsymbol{U} + \boldsymbol{C}_e^H\boldsymbol{B}_e\frac{d\boldsymbol{A}_e}{d\rho_m}\boldsymbol{H}_e\boldsymbol{U} + \boldsymbol{C}_e^H\boldsymbol{B}_e\boldsymbol{A}_e\boldsymbol{H}_e\frac{d\boldsymbol{U}}{d\rho_m} \tag{30}$$

where $\boldsymbol{B}_e$ is the strain-displacement matrix of the e-th element of the mesh, calculated at the centroid of the element, $\boldsymbol{H}_e$ is a localization matrix, which does the mapping between the global and local vectors and $\boldsymbol{A}_e$ is a matrix used to include the information of the incompatible modes into the problem.

With all the definitions, the final Augmented Lagrangian form is

$$\begin{aligned}\frac{d\mathscr{L}}{d\rho_m} &= \sum_{e=1}^{n} a_e\left\{\frac{d\boldsymbol{F}_e^T}{d\rho_m}\boldsymbol{\sigma}_e + \boldsymbol{F}_e^T\left(\frac{d\boldsymbol{C}_e^H}{d\rho_m}\boldsymbol{B}_e\boldsymbol{A}_e\boldsymbol{H}_e\boldsymbol{U} + \boldsymbol{C}_e^H\boldsymbol{B}_e\frac{d\boldsymbol{A}_e}{d\rho_m}\boldsymbol{H}_e\boldsymbol{U} + \boldsymbol{C}_e^H\boldsymbol{B}_e\boldsymbol{A}_e\boldsymbol{H}_e\frac{d\boldsymbol{U}}{d\rho_m}\right)\right.\\
&+ \left. 2\boldsymbol{\sigma}_e^T\boldsymbol{M}_e\left(\frac{d\boldsymbol{C}_e^H}{d\rho_m}\boldsymbol{B}_e\boldsymbol{A}_e\boldsymbol{H}_e\boldsymbol{U} + \boldsymbol{C}_e^H\boldsymbol{B}_e\frac{d\boldsymbol{A}_e}{d\rho_m}\boldsymbol{H}_e\boldsymbol{U} + \boldsymbol{C}_e^H\boldsymbol{B}_e\boldsymbol{A}_e\boldsymbol{H}_e\frac{d\boldsymbol{U}}{d\rho_m}\right) + \boldsymbol{\sigma}_e^T\frac{d\boldsymbol{M}_e}{d\rho_m}\boldsymbol{\sigma}_e\right\}\\
&+ \boldsymbol{\lambda}^T\frac{d\boldsymbol{K}}{d\rho_m}\boldsymbol{U} + \boldsymbol{\lambda}^T\boldsymbol{K}\frac{d\boldsymbol{U}}{d\rho_m} + V_m\frac{df_v^m}{d\rho_m},\end{aligned} \tag{31}$$

where

$$a_e = r\left\langle \frac{\mu_e}{r} + \Phi_e - 1 \right\rangle. \tag{32}$$

In order to avoid the costly evaluation of the derivatives of the displacement field, the problem is divided in two. The vector, $\boldsymbol{\lambda}$ is obtained through the auxiliary problem given by

$$\sum_{e=1}^{n} a_e\left\{\left(\boldsymbol{F}_e^T + 2\boldsymbol{\sigma}_e^T\boldsymbol{M}_e\right)\boldsymbol{C}_e^H\boldsymbol{B}_e\boldsymbol{A}_e\boldsymbol{H}_e\right\} + \boldsymbol{\lambda}^T\boldsymbol{K} = \boldsymbol{0}^T \tag{33}$$

and it is used in the direct problem, given by,

$$\begin{aligned}\frac{d\mathscr{L}}{d\rho_m} &= V_m\frac{df_v^m}{d\rho_m}+a_m\left\{\frac{d\boldsymbol{F}_m^T}{d\rho_m}\boldsymbol{\sigma}_m+\boldsymbol{F}_m^T\left(\frac{d\boldsymbol{C}_m^H}{d\rho_m}\boldsymbol{B}_m\boldsymbol{A}_m\boldsymbol{F}_m\boldsymbol{U}+\boldsymbol{C}_m^H\boldsymbol{B}_m\frac{\boldsymbol{A}_m}{d\rho_m}\boldsymbol{H}_m\boldsymbol{U}\right)\right.\\ &+ \left.2\boldsymbol{\sigma}_m^T\boldsymbol{M}_m\left(\frac{d\boldsymbol{C}_m^H}{d\rho_m}\boldsymbol{B}_m\boldsymbol{A}_m\boldsymbol{H}_m\boldsymbol{U}+\boldsymbol{C}_m^H\boldsymbol{B}_m\frac{d\boldsymbol{A}_m}{d\rho_m}\boldsymbol{H}_m\boldsymbol{U}\right)+\boldsymbol{\sigma}_m^T\frac{d\boldsymbol{M}_m}{d\rho_m}\boldsymbol{\sigma}_m\right\}\\ &+ \boldsymbol{\lambda}^T\frac{d\boldsymbol{K}}{d\rho_m}\boldsymbol{U}\end{aligned} \tag{34}$$

in order to evaluate the derivatives of the Augmented Lagrangian function. The derivatives of the stiffness matrix can be obtained by

$$\frac{d\boldsymbol{K}}{d\rho_m}=\int_\Omega \boldsymbol{B}^T\frac{d\boldsymbol{C}}{d\rho_m}\boldsymbol{B}d\Omega, \tag{35}$$

and the derivatives of the fourth order elasticity tensor can be obtained analytically by equations 8, 9 and 10. The derivatives of the volume fraction of the m-th element of the mesh can be obtained analytically through equation 11.

4. Preliminary Result

The optimal design of a cantilever beam with distributed load is used in to investigate the behaviour of the proposed formulation. Figure 5 shows a side view of the design domain which is discretized with $50\times10\times10$ finite elements for an initial study. Thus, there are 10×10^3 design variables and 5×10^3 stress constraints.

Figure 5. Cantilever beam with distributed load (side view).

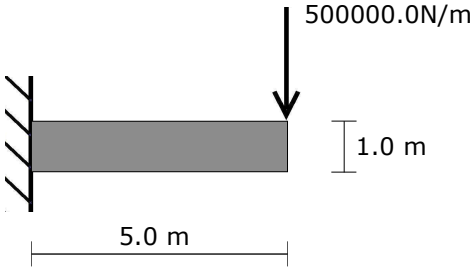

The initial penalty parameter used is given by

$$r=10\frac{V_0(\boldsymbol{\rho}_0)}{\sum_e\langle g_e^0(\boldsymbol{\rho}_0)\rangle}, \tag{36}$$

where V_0 is the initial volume of the structure, $\boldsymbol{\rho}_0$ is the initial distribution of design variables and g_e^0 is the initial constraint associated to the e-th element of the mesh.

The penalty parameter is updated by 10% when the internal loop of the algorithm reaches its optimum value. The algorithm stops when all constraints are satisfied and the present inner loop reaches the optimum value. The initial Lagrange multipliers are set as zero and are updated, for the e-th element at k-th iteration, in each external iteration as

$$\mu_e^k=\left\langle\mu_e^{k-1}+r\left(\Phi_e^k-1\right)\right\rangle. \tag{37}$$

In order to maintain a smooth spatial variation between the design variables, both the external and the internal diameters are filtered. The length of the filter is $0.2m$.

Figures 6 and 7 show the spatial distribution of the design variables of the problem, the external and internal diameters of the hollow spheres, respectively. It can be seen that the distribution of both diameters are smooth, showing that the filtering scheme adopted is efficient. In order to make the interpretation of the result easier, figure 8 shows the distribution of the volume fraction in each finite element on the optimal solution.

Figure 9 shows the spatial variation of the Tsai-Wu criteria in the optimal solution. As it can be seen, the failure criteria is not violated.

Figure 6. Optimal distribution of ρ_o.

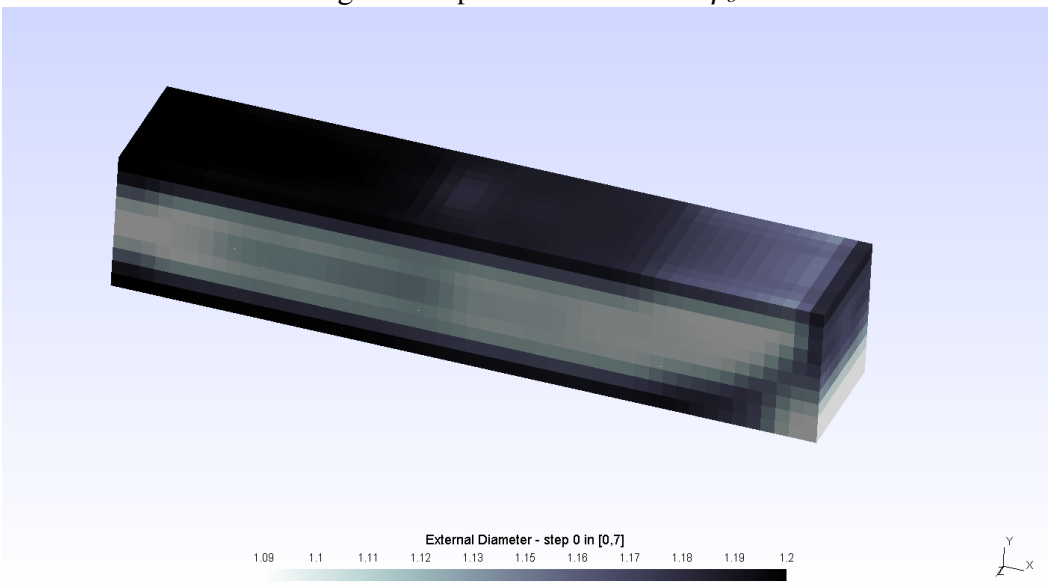

Figure 7. Optimal distribution of ρ_i.

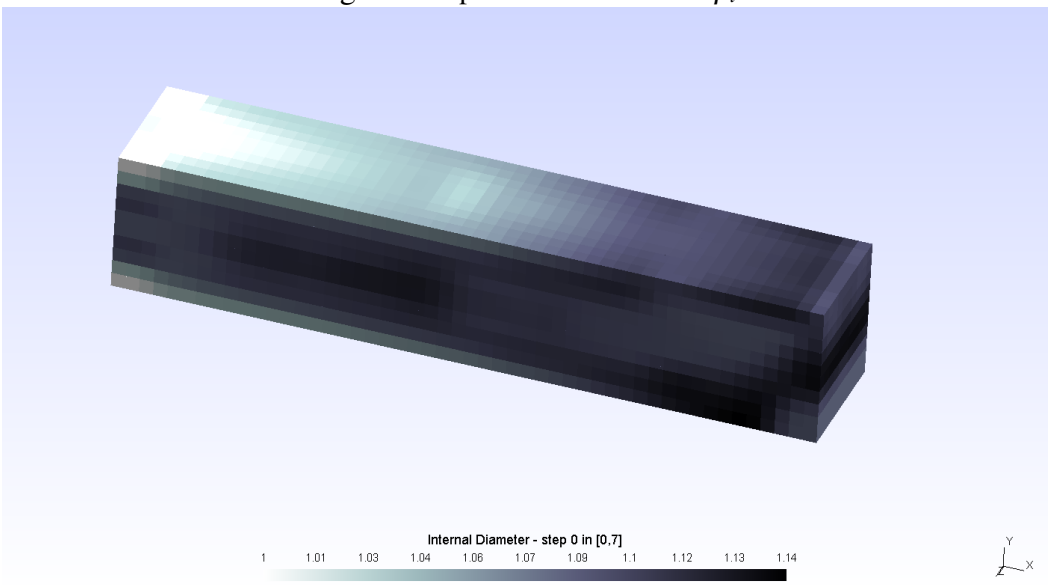

Figure 8. Optimal distribution of f_v.

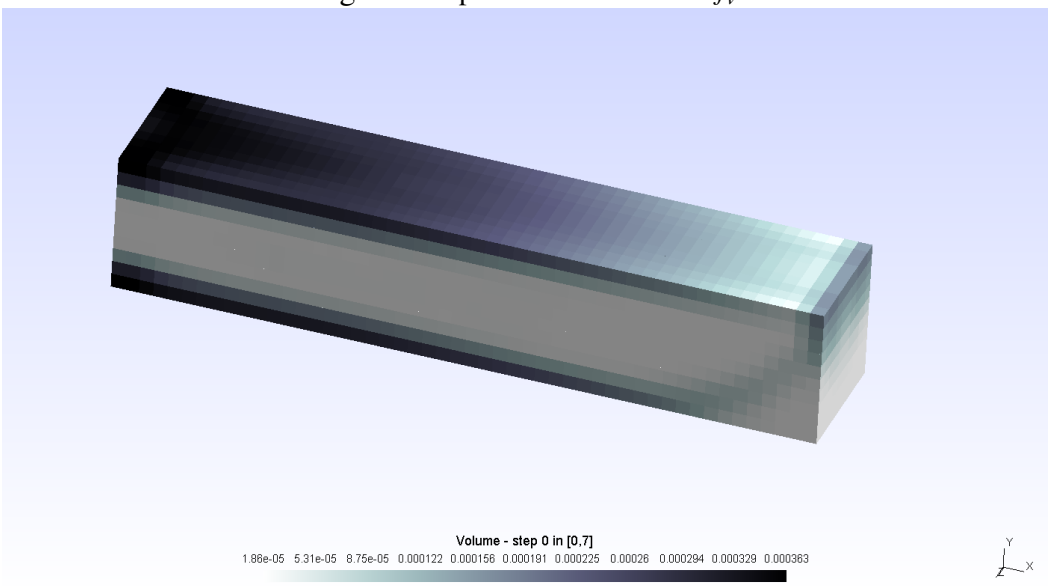

Figure 9. Optimal distribution of Φ.

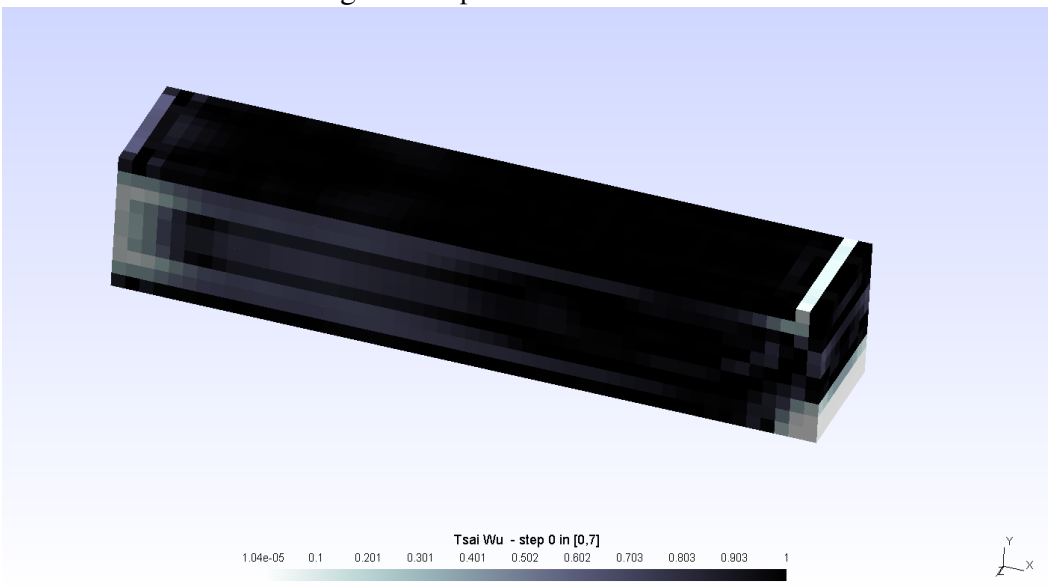

Figure 10 shows the convergence of the Augmented Lagrangian function in each internal iteration of the algorithm. The first changes in the external loop are clearly seen in the discontinuities in the convergence. This is explained by the form of the Augmented Lagrangian function, equation 24. In the first iteration, several constraints are active and represent a significant contribution in the objective function. In the further iterations, the convergence becomes smoother and the tendency is that all the constraint became inactive, rendering the Augmented Lagrangian function the volume of the structure.

Figure 10. Convergence of Augmented Lagrangian function

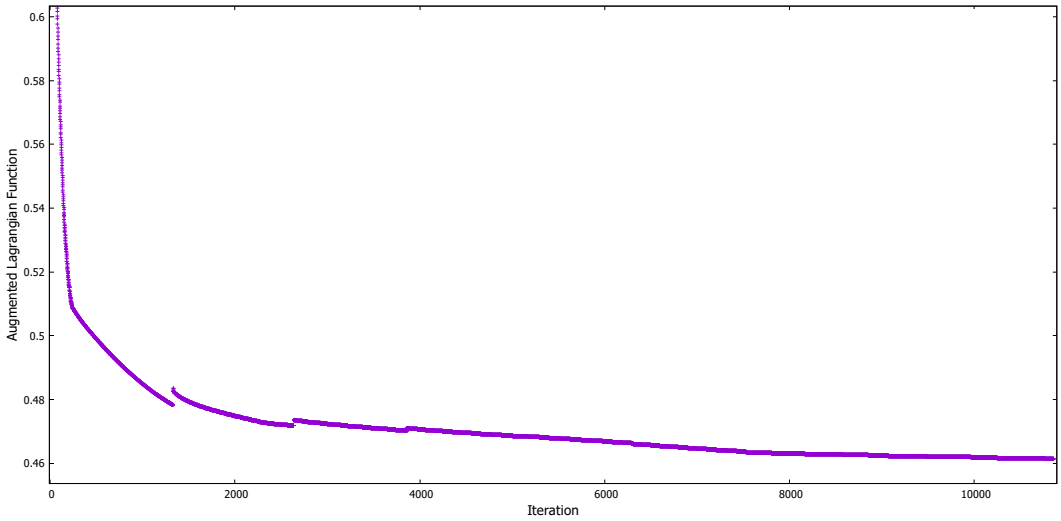

Figure 11 shows the convergence of the Maximum value of Tsai Wu criteria in each internal iteration. Again, it can be seen, in the first iterations, the change in the external loop of the algorithm, represented by the regions where the convergence became more pronounced. In further iterations, the value of the constraint increasingly comes closer to zero, rendering the convergence curve smoother.

Figure 11. Convergence of the Maximum value of Tsai-Wu failure Criteria

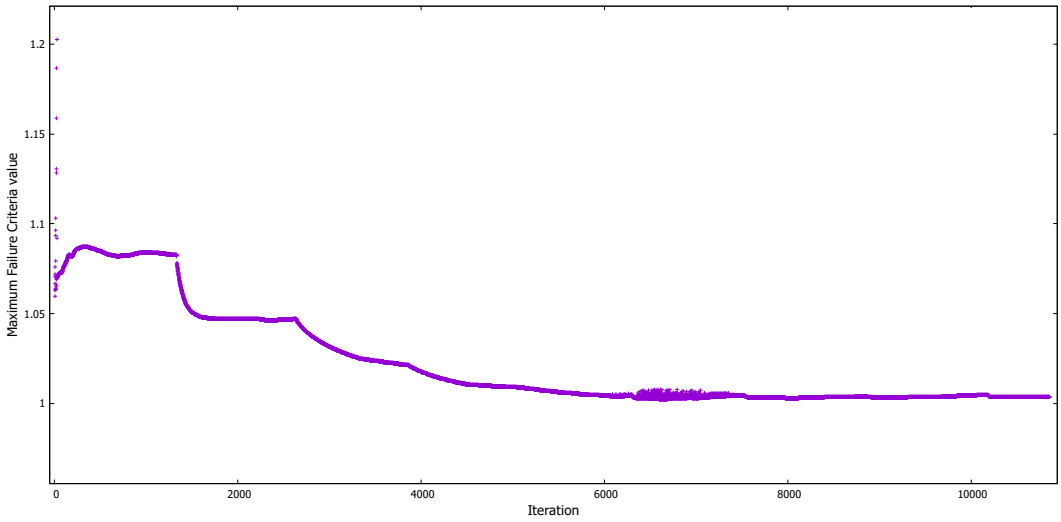

It is interesting to note that for small volume fractions, the influence of the Tsai-Wu strength coefficients are more important than the value of the effective stress at the point. Figure 12 shows the ratio between C^H_{1111} and X^t_1 with respect to the volume fraction, for $\rho_o = 1.2$. Thus, using an 1D model as reference (where the stress is directly proportional to C^H_{1111} and X^t_1 is the only strength parameter) it can be seen that the optimization depends on a non obvious trend between the design variables. Also, as the obtained parameterization resembles the relaxed stress parameterization obtained with the qp approach [21], there is no need to impose an artificial relaxation.

Figure 12. C^H_{1111}/X^t_1 with respect to the effective volume fraction, for $\rho_o = 1.2$

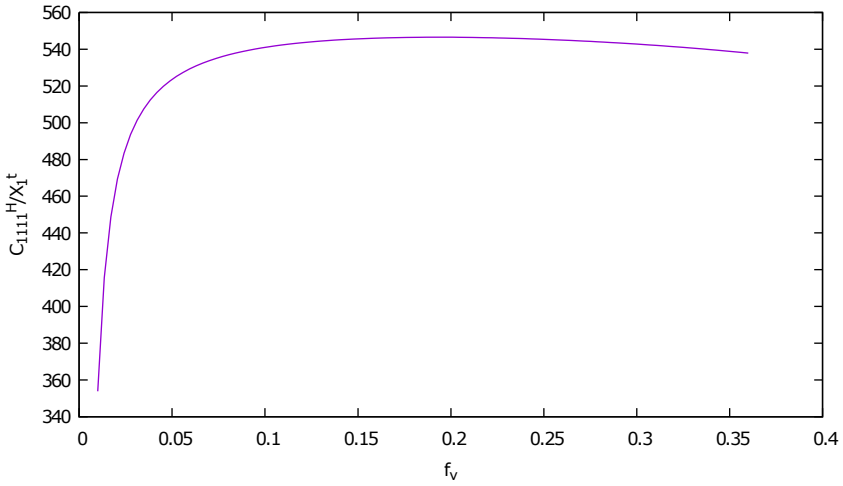

5. Conlusion

This work addresses the optimal design of lightweight structures made of a hollow-sphere material. To this end, the geometry of the micro structure is described by two design variables and the homogenization by asymptotic approach is used to obtain the effective tensor of elastic properties. The effective strength properties are modelled by the Tsai-Wu stress criteria, where the material coefficients are obtained by simulating a tensile and a shear test on this material.

The preliminary results show that the parameterization used and the optimization strategy are consistent. The common singularity problem associated to stress constrains in the traditional SIMP parameterization is avoided since the parameterization is based in a consistent micro mechanical model.

With this model, it is possible to adjust different mechanical behaviours in traction, shear and compression.

REFERENCES

[1] Ochsner, A., Hosseini, S. M. H., and Merkel, M. (2009). "Numerical Simulation of Sintered Perforated Hollow Sphere Structures (PHSS) to Investigate Thermal Conductivity." In Proceedings of the International MultiConference of Engineers and Computer Scientists, volume 2.

[2] Sanders, W. and Gibson, L. (2003). "Mechanics of hollow sphere foams." Materials Science and Engineering: A, 347(1):70–85.

[3] Hollister, S. J. and Kikuchi, N. (1992). "A comparison of homogenization and standard mechanics analyses for periodic porous composites." Computational Mechanics, 10(2):73–95.

[4] Hollister, S. J. and Kikuchi, N. (1994). "Homogenization theory and digital imaging: a basis for studying the mechanics and design principles of bone tissue." Biotechnology and bioengineering, 43(7):586–596.

[5] Sanchez-Palencia, E. (1986). "Homogenization in mechanics. A survey of solved and open problems." Rend. Sem. Mat. Univ. Politec. Torino, 44(1):1–45.

[6] Guedes, J. and Kikuchi, N. (1990). "Preprocessing and postprocessing for materials based on the homogenization method with adaptive finite element methods." Computer methods in applied mechanics and engineering, 83(2):143–198.

[7] Hassani, B. and Hinton, E. (1998). "A review of homogenization and topology optimization I - homogenization theory for media with periodic structure." Computers & Structures, 69(6):707–717.

[8] Hassani, B. and Hinton, E. (1998). "A review of homogenization and topology opimization II - analytical and numerical solution of homogenization equations." Computers & structures, 69(6):719–738.

[9] Fang, Z., Sun, W., and Tzeng, J. T. (2004). "Asymptotic homogenization and numerical implementation to predict the effective mechanical properties for electromagnetic composite conductor." Journal of Composite Materials, 38(16):1371–1385.

[10] Hughes, T. J. (2012). The finite element method: linear static and dynamic finite element analysis. Courier Corporation.

[11] Olakanmi, E., Cochrane, R., and Dalgarno, K. (2015). "A review on selective laser sintering/melting (SLS/SLM) of aluminium alloy powders: Processing, microstructure, and properties." Progress in Materials Science, 74:401–477.

[12] Tsai, S. W. and Wu, E. M. (1971). "A general theory of strength for anisotropic materials." Journal of composite materials, 5(1):58–80.

[13] Hahn, H. T. and Tsai, S. W. (1980). Introduction to composite materials. CRC Press.

[14] de Medeiros, R., Rodriguez-Ramos, R., Guinovart-Diaz, R., Bravo-Castillero, J., Otero, J. A., and Tita, V. (2015). "Numerical and analytical analyses for active fiber composite piezoelectric composite materials." Journal of Intelligent Material Systems and Structures, 26(1):101–118.

[15] Medeiros, R. D., Moreno, M. E., Marques, F. D., and Tita, V. (2012). "Effective properties evaluation for smart composite materials." Journal of the Brazilian Society of Mechanical Sciences and Engineering, 34:362–370.

[16] Brito-Santana, H., De Medeiros, R., Rodriguez-Ramos, R., and Tita, V. (2016). "Different interface models for calculating the effective properties in piezoelectric composite materials with imperfect fiber-matrix adhesion." Composite Structures, 151:70–80.

[17] Rodriguez-Ramos, R., de Medeiros, R., Guinovart-Díaz, R., Bravo-Castillero, J., Antonio Otero, J., and Tita, V. (2013). "Different approaches for calculating the effective elastic properties in composite materials under imperfect contact adherence." 99:264–275.

[18] Bruns, T. E. and Tortorelli, D. A. (2001). "Topology optimization of non-linear elastic structures and compliant mechanisms." Computer Methods in Applied Mechanics and Engineering, 190(26):3443–3459.

[19] Sigmund, O. (2007). "Morphology-based black and white filters for topology optimization." Structural and Multidisciplinary Optimization, 33(4-5):401–424.

[20] da Silva, G. and Cardoso, E. (2017). "Stress-based topology optimization of continuum structures under uncertainties." Computer Methods in Applied Mechanics and Engineering, 313:647–672.

[21] Bruggi, M. (2008). "On an alternative approach to stress constraints relaxation in topology optimization." Structural and Multidisciplinary Optimization, 36(2):125–141. ISSN 1615-1488. doi:10.1007/s00158-007-0203-6.

RESPONSIBILITY NOTICE

The authors are the only responsible for the printed material included in this paper.